AGU ADVANCING EARTH AND SPACE SCIENCE

Geophysical Research Letters

RESEARCH LETTER
10.1029/2020GL090861

Key Points:

- We examine the response of the climate system to abrupt 1.5×, 2×, 3×, 4×, 5×, 6×, 7×, and 8×CO_2 forcing with two different coupled models
- Climate sensitivity, sea-ice extent, global precipitation and the atmospheric circulation respond non-monotonically across this range of CO_2
- The non-monotonicity of the response is associated with changes in ocean dynamics, notably over the North Atlantic

Supporting Information:

- Supporting Information S1

Correspondence to:
I. Mitevski,
im2527@columbia.edu

Citation:
Mitevski, I., Orbe, C., Chemke, R., Nazarenko, L., & Polvani, L. M. (2021). Non-monotonic response of the climate system to abrupt CO_2 forcing. *Geophysical Research Letters*, *48*, e2020GL090861. https://doi.org/10.1029/2020GL090861

Received 21 SEP 2020
Accepted 28 FEB 2021

Non-Monotonic Response of the Climate System to Abrupt CO_2 Forcing

Ivan Mitevski[1], Clara Orbe[2], Rei Chemke[1], Larissa Nazarenko[2,3], and Lorenzo M. Polvani[1,4]

[1]Department of Applied Physics and Applied Mathematics, Columbia University, New York, NY, USA, [2]NASA Goddard Institute for Space Studies, New York, NY, USA, [3]Center for Climate System Research, Columbia University, New York, NY, USA, [4]Lamont-Doherty Earth Observatory, Columbia University, Palisades, NY, USA

Abstract We explore the climate system response to abrupt CO_2 forcing, spanning the range 1× to 8×CO_2, with two state-of-the-art coupled atmosphere-ocean-sea-ice-land models: the NASA Goddard Institute for Space Studies Model E2.1-G (GISS-E2.1-G) and the Community Earth System Model (CESM-LE). We find that the effective climate sensitivity is a non-monotonic function of CO_2 in both models, reaching a minimum at 3×CO_2 for GISS-E2.1-G, and 4×CO_2 for CESM-LE. A similar non-monotonic response is found in Northern Hemisphere surface temperature, sea-ice, precipitation, the latitude of zero precipitation-minus-evaporation, and the strength of the Hadley cell. Interestingly, the Atlantic meridional overturning circulation collapses when non-monotonicity appears and does not recover for larger CO_2 forcings. Analyzing the climate response over the same CO_2 range with slab-ocean versions of the same models, we demonstrate that the climate system's non-monotonic response is linked to ocean dynamics.

Plain Language Summary We perform runs with two different models using CO_2 concentrations in the atmosphere higher (from 1× to 8×CO_2) relative to pre-industrial conditions, in order to explore how the effective climate sensitivity (ECS_{eff}) and the entire climate system change with increasing CO_2. We show that ECS_{eff} is a non-monotonic function of CO_2, minimizing at 3×CO_2 in one model and 4×CO_2 in the other. A similar non-monotonic response appears in precipitation, sea-ice, the edge of the dry zone, and Hadley cell strength. Interestingly, the Atlantic Meridional Overturning Circulation, which brings warm water into the North Atlantic, also shuts down at the same forcings when ECS_{eff} is minimum and does not recover for higher forcings. We further show that the non-monotonic response of the climate system stems from changes in ocean dynamics.

1. Introduction

Equilibrium Climate Sensitivity (ECS) is the global mean surface warming at equilibrium following an instantaneous doubling of CO_2 relative to pre-industrial (PI) conditions (Knutti et al., 2017). It is among the most important metrics in climate science, and is widely used in economic and policy assessments of future global warming. Due to the complexity of the climate system, however, ECS is poorly constrained and its uncertainty has not narrowed across the reports of the Intergovernmental Panel on Climate Change (IPCC), from 1.9–5.2 K in the first to 1.5–4.5 K in the fifth report (Knutti & Hegerl, 2008; Knutti et al., 2017; Tian, 2015). ECS estimates from the Coupled Model Intercomparison Project 6 (CMIP6) span a still larger range of values (1.8–5.6 K) (Zelinka et al., 2020). Analyzing individual feedback processes, in addition to both historical and paleoclimate records, a recent ECS assessment shows a 66% range spanning 2.6–3.9 K (Sherwood et al., 2020).

Part of the difficulty in reducing ECS uncertainty is that it remains unclear to what degree ECS is a function of CO_2 concentration. Thus, while ECS estimates inferred from historical (observed) warming are lower than the ECS estimates derived from models subjected to abrupt CO_2 forcing (Knutti et al., 2017; Marvel et al., 2018), this does not necessarily imply that the model estimates are biased high. Comparisons of ECS derived from paleoclimate reconstructions also produce mixed results when compared with general circulation models (GCMs). While some paleoclimate studies indicate that climate sensitivity changes with CO_2 concentration (Friedrich et al., 2016; Shaffer et al., 2016; Stap et al., 2019), others do not (Martínez-Botí

et al., 2015). In contrast, for the present and future climate most GCM studies show that ECS increases with CO_2 (Caballero & Huber, 2013; Colman & McAvaney, 2009; Gregory et al., 2015; Jonko et al., 2013; Meraner et al., 2013). Of particular interest here, Meraner et al. (2013) showed that effective climate sensitivity (ECS_{eff}) increases monotonically in warmer climates, growing from 2.79 K for an abrupt 2×CO_2 forcing to 10.22 K for a 16×CO_2 forcing. However, that result was obtained using a single slab-ocean model, and whether it holds in the presence of a dynamically active ocean is still an open question.

Going beyond ECS, O'Gorman and Schneider (2008) explored the hydrological cycle response to increasing CO_2 using an idealized GCM, and reported a non-monotonic response in large-scale global mean precipitation with surface temperature. Idealized models also suggest that the Hadley cell (HC) strength responds non-monotonically to surface temperature, reaching a maximum value near present-day climate (Levine & Schneider, 2011; O'Gorman & Schneider, 2008). Studies with comprehensive models have also found that the width of the tropics will widen with increased warming (Chemke & Polvani, 2019; Grise et al., 2019), but the question of whether the widening is monotonic over a wide range of CO_2 forcing in a comprehensive coupled climate model remains unexplored.

Here we perform a series of abrupt CO_2 model runs using the coupled atmosphere-ocean-sea-ice-land NASA Goddard Institute for Space Studies ModelE (GISS-E2.1-G) (Kelley et al., 2020), and Community Earth System Model Large Ensemble (CESM-LE, Kay et al., 2015), to quantify the response of the climate system over an extensive range of CO_2 forcings (1× to 8×CO_2). Extending the work of Meraner et al. (2013), we explore the fully coupled atmosphere-ocean system (not only the slab-ocean system), and we go beyond ECS_{eff} to analyze the response of many other important components of the climate system, notably sea-ice, precipitation, and the HC. As shown below, we find the response for many such components to be not only a non-linear but *a non-monotonic* function of CO_2 forcing in both the GISS and CESM models.

2. Methods

We use fully coupled atmosphere-ocean-sea-ice-land (FOM) and the slab-ocean (SOM) versions of GISS-E2.1-G and CESM-LE. In the FOM version of GISS-E2.1-G, a 40-level atmospheric model with a resolution of 2° × 2.5° latitude/longitude is coupled to the 1° horizontal resolution 40-level GISS Ocean v1 (GO1) model: this model configuration contributed to the CMIP6 project, and is denoted as "GISS-E2-1-G, r1i1p1f1." In the SOM version, the same atmospheric model is coupled to a mixed-layer ocean, with a prescribed ocean heat transport (OHT) derived from an atmosphere-only PI integration constrained with observed PI sea surface temperatures (Schmidt et al., 2006). The FOM of CESM-LE uses the Community Earth System Model version 1 (CESM1), the Community Atmosphere Model version 5 (CAM5, 30 vertical levels), and parallel ocean program version 2 (POP2, 60 vertical levels) with approximately 1° horizontal resolution in all model components (Kay et al., 2015). The SOM configuration of CESM-LE uses the same atmospheric model coupled to a mixed-layer ocean with prescribed OHT (Bitz et al., 2012), kept constant at PI annual and monthly values of CESM, respectively.

For the FOM versions, we perform a series of abrupt CO_2 forcing runs, with 1.5× (only GISS-E2.1-G), 2×, 3×, 4×, 5×, 6×, 7×, and 8×CO_2 forcings, with all other trace gases, ozone concentrations, and aerosols fixed at PI values. We contrast these to a PI control run. To clarify: we are not progressively doubling CO_2, as done in some other studies, but we start each forced run from PI conditions. Following the 4×CO_2 protocol for CMIP6, all of our abrupt CO_2 model runs are integrated for 150 years starting from PI conditions.

In addition to the FOM runs, we also carry out 60-year-long integrations with the SOM version of the models for 2×, 3×, and 4×CO_2 forcings, and contrast them to a 60-year-long PI control run.

Following Forster et al. (2016), we estimate the effective radiative forcing (ERF_{fSST}) by performing 30-year-long integrations using prescribed pre-industrial sea surface temperatures (SST) and sea ice. As in the FOM simulations, these are performed for 1.5× (only for GISS-E2.1-G), 2×, 3×, 4×, 5×, 6×, 7×, and 8×CO_2. The ERF_{fSST} is then calculated as the difference in global mean net top of the atmosphere (TOA) flux be-

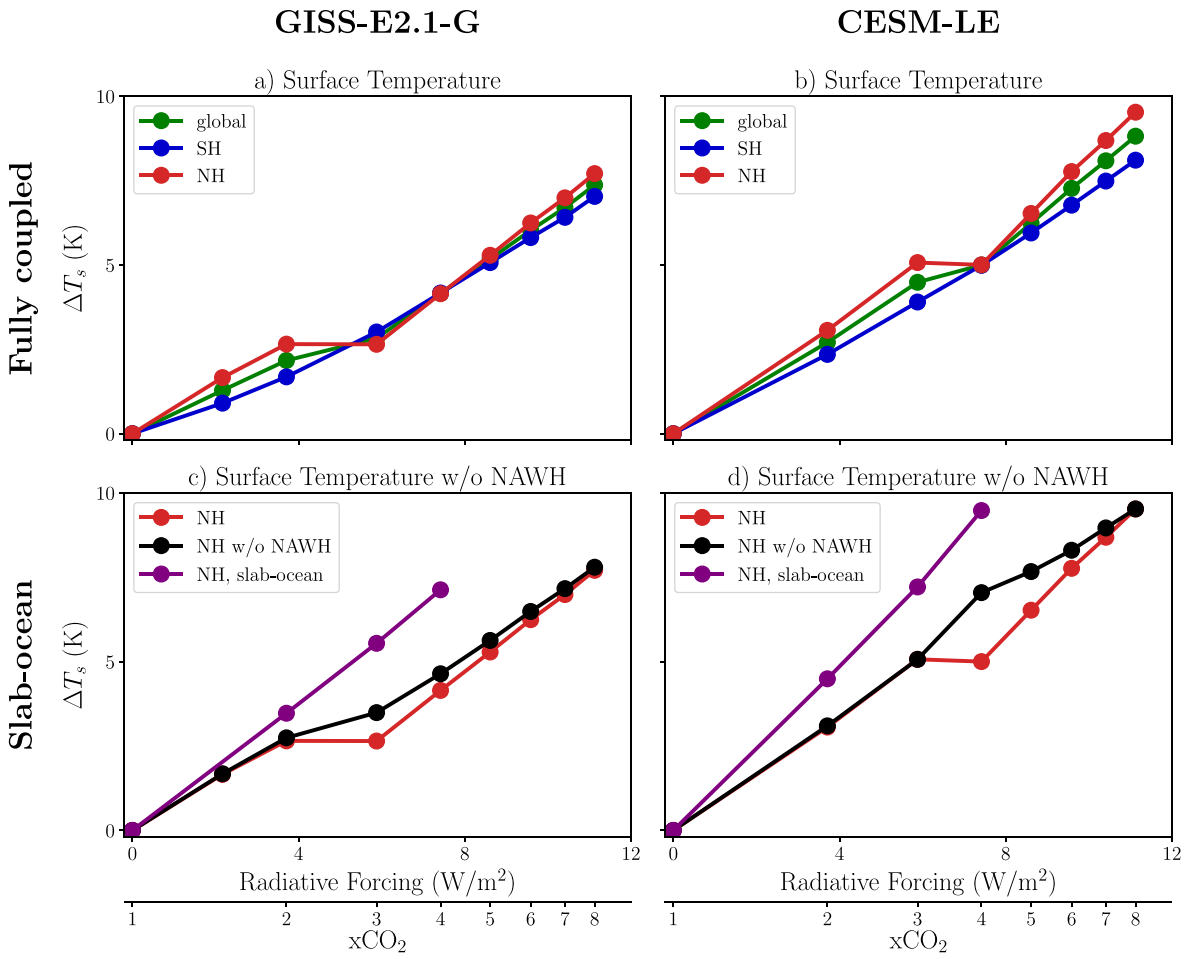

Figure 1. Annual surface temperature response (ΔT_s) as a function of radiative forcing in (a and b) fully coupled model (FOM) runs for the global mean (green), NH (red), and SH (blue), and (c and d) for the NH with (red) and without the North Atlantic Warming Hole (NAWH, black) and slab-ocean (SOM) runs (purple). Panels (a and c) show GISS-E2.1-G data and panels (b and d) show CESM-LE data. CESM-LE, Community Earth System Model Large Ensemble; GISS-E2.1-G, Goddard Institute for Space Studies Model E2.1-G; NH, Northern Hemisphere; SH, Southern Hemisphere.

tween PI and $n\times CO_2$, and it includes the adjustments of both the stratosphere and troposphere (Sherwood et al., 2015).

Following Meraner et al. (2013), we consider the Earth's energy balance in response to an abrupt CO_2 forcing in terms of

$$\Delta R = F + \lambda \Delta T \tag{1}$$

where F is the radiative forcing, ΔR is the TOA radiative imbalance, ΔT is the surface temperature response, and λ is the total feedback parameter. ECS_{eff}, defined as the temperature response when $\Delta R = 0$, is then calculated from the simple formula $ECS_{eff} = -F/\lambda$.

For each run, we perform a regression analysis (Gregory et al., 2004) of ΔR versus ΔT, using annual mean values, to calculate total radiative feedbacks (λ, slope) and the effective radiative forcing (ERF_{reg}, y-intercept). We then evaluate the effective climate sensitivity, $ECS_{eff} = -ERF_{fSST,2xCO_2} / \lambda$, where $ERF_{fSST,2xCO_2}$ is the ERF_{fSST} estimated from the $2\times CO_2$ fixed SST experiment.

In addition to the global mean surface temperature response, we examine the response of precipitation, sea-ice extent, the width of the tropical belt, and the strength of the Atlantic Meridional Overturning Circulation (AMOC, defined as the maximum between 30°N to 55°N and 800–2,000m). To quantify the tropical width, we use the edge of the dry zones, ϕ_{P-E}, defined as the latitude where precipitation (P) minus evapo-

Table 1
Total Feedbacks λ [$Wm^{-2}K^{-1}$] (Slope in Gregory Regression Plot), Effective Climate Sensitivity (ECS_{eff}) Calculated as $-ERF_{fSST,2xCO_2} / \lambda$ [K] With $ERF_{fSST,2xCO_2}$ Being 3.63 Wm^{-2} for GISS-E2.1-G and 3.88 Wm^{-2} for CESM-LE Model, and Global Surface Temperature Response ΔT_s [K]

	1.5×CO_2	2×CO_2	3×CO_2	4×CO_2	5×CO_2	6×CO_2	7×CO_2	8×CO_2
GISS-E2.1-G								
λ_F	−1.72 (−1.89, −1.56)	−1.62 (−1.77, −1.47)	−1.86 (−2.06, −1.72)	−1.51 (−1.63, −1.39)	−1.35 (−1.44, −1.24)	−1.26 (−1.34, −1.15)	−1.24 (−1.31, −1.14)	−1.22 (−1.29, −1.12)
$ECS_{eff,F}$	2.11 (1.92, 2.34)	2.24 (2.05, 2.46)	1.95 (1.76, 2.11)	2.41 (2.23, 2.60)	2.69 (2.51, 2.92)	2.89 (2.71, 3.14)	2.93 (2.77, 3.19)	2.99 (2.82, 3.24)
$\Delta T_{s,F}$	1.28 (1.24, 1.32)	2.17 (2.12, 2.22)	2.83 (2.78, 2.88)	4.16 (4.11, 4.21)	5.18 (5.13, 5.23)	6.03 (5.98, 6.08)	6.70 (6.65, 6.75)	7.36 (7.31, 7.41)
λ_S	-	−1.30 (−1.40, −1.24)	−1.22 (−1.28, −1.15)	−1.20 (−1.24, −1.13)	-	-	-	-
$ECS_{eff,S}$	-	2.80 (2.62, 2.93)	2.97 (2.84, 3.16)	3.04 (2.92, 3.22)	-	-	-	-
$\Delta T_{s,S}$	-	3.13 (3.10, 3.16)	4.99 (4.97, 5.01)	6.43 (6.41, 6.45)	-	-	-	-
CESM-LE								
λ_F	-	−1.08 (−1.20, −0.94)	−0.99 (−1.08, −0.88)	−1.25 (−1.31, −1.17)	−1.10 (−1.18, −1.00)	−1.03 (−1.11, −0.92)	−0.97 (−1.05, −0.89)	−0.97 (−1.04, −0.88)
$ECS_{eff,F}$	-	3.60 (3.23, 4.11)	3.95 (3.59, 4.43)	3.11 (2.96, 3.32)	3.53 (3.30, 3.88)	3.79 (3.51, 4.21)	4.00 (3.70, 4.38)	3.99 (3.73, 4.39)
$\Delta T_{s,F}$	-	2.70 (2.64, 2.77)	4.47 (4.40, 4.55)	4.99 (4.90, 5.07)	6.22 (6.09, 6.35)	7.25 (7.12, 7.38)	8.06 (7.94, 8.18)	8.79 (8.67, 8.91)
λ_S	-	−0.80 (−0.91, −0.66)	−0.83 (−0.89, −0.77)	−0.82 (−0.89, −0.72)	-	-	-	-
$ECS_{eff,S}$	-	4.90 (4.30, 5.79)	4.66 (4.35, 5.03)	4.74 (4.36, 5.35)	-	-	-	-
$\Delta T_{s,S}$	-	4.00 (3.96, 4.05)	6.37 (6.32, 6.42)	8.32 (8.28, 8.35)	-	-	-	-

Note: ^{F}Fully coupled (FOM); ^{S}Slab-ocean (SOM).
All confidence intervals (CIs) are 95%; CIs for λ and ECS_{eff} are obtained by resampling the linear regressions 10,000 times, and CIs for ΔT are calculated using Student's *t*-distribution.

ration (E) is zero poleward of the subtropical minimum and equatorward of 60° (see Figure 1 in Grise and Polvani, 2016). We calculate ϕ_{P-E} using the tropical-width diagnostics (TropD) code documented in Adam et al. (2018) by applying the "zero_crossing" method.

Finally, in all figures below we show the average over the last 50 years of the FOM runs and of the last 30 years of the SOM runs. For all quantities of interest, the annual mean response (denoted by Δ) is computed as the difference from the corresponding PI control run. The linearity of various climate metrics is evaluated with respect to the radiative forcing (RF) associated with each CO_2 perturbation, calculated from the expression $5.35\ln(n \times CO_2/1 \times CO_2)$ (Byrne & Goldblatt, 2014) where, for each run, n is the CO_2 multiple of the PI value. Note that, upon comparing this logarithmic RF value to ERF_{fSST} and ERF_{reg}, we find values that are very close to ERF_{fSST} and relatively close to ERF_{reg} (see Figure S1).

3. Results

Table 1 summarizes the Gregory regression analysis for all CO_2 integrations for both FOM and SOM configurations (the individual regression plots for each run are shown in Figure S2). Feedbacks in the FOM runs (denoted λ_F, Table 1, rows 1,7) initially increase (i.e., become less negative) with rising CO_2, but reach a minimum (maximum of $|\lambda_F|$) value at 3×CO_2 for GISS-E2.1-G and 4×CO_2 for CESM-LE. More precisely, for GISS-E2.1-G, λ_F becomes more positive from 1.5× to 2×CO_2 (−1.72 to −1.62), reaches an absolute minimum at 3×CO_2 ($\lambda_F = -1.86$), and then monotonically increases to a value of −1.22 at 8×CO_2. In other words, $ECS_{eff,F}$, which is inversely related to λ_F, reaches an absolute minimum (1.95) at 3×CO_2 for the FOM version of GISS-E2.1-G (Table 1, row 2). Similarly, for CESM-LE, λ_F becomes more positive from 2× to 3×CO_2 (−1.08 to −0.99), reaches an absolute minimum at 4×CO_2 ($\lambda_F = -1.25$), and then monotonically increases

to a value of −0.97 at 8×CO_2. $ECS_{eff,F}$ also reaches an absolute minimum (3.11) at 4×CO_2 for the FOM run (Table 1, row 8).

In contrast to the FOM runs, the SOM integrations do not show this non-monotonicity for either model. Rather, the feedbacks in the SOM runs (denoted λ_S, Table 1, rows 4,10) increase monotonically from 2× to 4×CO_2 (the difference between 3× and 4×CO_2 in CESM-LE runs is not statistically significant). Correspondingly, $ECS_{eff,S}$, does not exhibit the minimum at 3×CO_2 for GISS-E2.1-G and 4×CO_2 for CESM-LE featured in the fully coupled runs. Our SOM results confirm the findings of Meraner et al. (2013), who also reported that ECS_{eff} increases monotonically with CO_2 concentrations using a SOM model. The monotonic behavior of ECS_{eff} with a SOM model clearly points to the ocean dynamics as key to understanding the non-monotonicity.

Next, going beyond the numerical value ECS, we examine several key aspects of the climate system response to increasing CO_2. The global mean surface temperature response ΔT_s (green lines in Figures 1a and 1b and Table 1, rows 3,9) is a monotonic function of RF, although one can see an inflection in NH surface temperatures at 3×CO_2 in GISS-E2.1-G and 4×CO_2 in CESM-LE. Partitioning ΔT_s into northern (red lines in Figures 1a and 1b) and southern (blue lines in Figures 1a and 1b) hemispheric mean components reveals a clear cooling in the northern hemisphere (NH) as the forcing is increased from 2× to 3×CO_2 for GISS-E2.1-G and 3× to 4×CO_2 for CESM-LE model (this corresponds to the ECS_{eff} minimum). In the southern hemisphere (SH), on the other hand, the surface temperature increases monotonically. The non-monotonic behavior in the NH surface temperature is absent in the SOM runs in both models (Figures 1c and 1d, purple lines). This again demonstrates that ocean dynamics is responsible for the non-monotonic behavior of the NH surface temperature.

Inspection of global maps of ΔT_s (see Figure 2) shows that the non-monotonicity in the coupled model run at 3×CO_2 for GISS-E2.1-G and 4×CO_2 for CESM-LE is associated with a non-monotonic response of the North Atlantic Warming Hole (NAWH), where there is a decline in SST in response to increasing greenhouse gases. To evaluate the contribution of this regional cooling to the total NH temperatures, we mask out all grid points corresponding to the NAWH, which we define here as regions where ΔT_s is negative (blue areas in Figure 2). The resulting ΔT_s (Figures 1c and 1d, black lines) is monotonic in NH as in the SOM runs. The latter, along with the behavior in the SOM runs, strongly suggests that changes in ocean dynamics are responsible for the non-monotonicity in NH surface temperature exhibited in the coupled model.

Recently, Chemke et al. (2020) showed that the formation of the NAWH in CESM-LE and the Max Planck Institute Earth System Model 100-member Grand Ensemble (MPI-GE) (Maher et al., 2019) under historical forcing from 1850 to 2005 and Representative Concentration Pathway 8.5 (RCP8.5) through 2100, is caused by a reduction in surface meridional OHT. Additionally, a reduction in the meridional overturning circulation (MOC) has been shown to reduce transient warming in numerous studies (Caesar et al., 2020; Palter, 2015; Rugenstein et al., 2013; Trossman et al., 2016; Winton et al., 2013). Thus, it is tempting to relate the AMOC response (which plays a central role in the poleward OHT) to the surface temperature response. This can be seen in Figures S3a and S3b: as CO_2 increases, the AMOC weakens, and the associated reduction in OHT is accompanied by the NAWH, which maximizes (relative to ambient global warming) at 3×CO_2 in GISS-E2.1-G and 4×CO_2 in CESM-LE (Figures 2c and 2f) when the AMOC entirely collapses. At higher forcings, 4× to 8×CO_2 for GISS-E2.1-G, and 5× to 8×CO_2 for CESM-LE, the AMOC remains shut down, but the surface warms as CO_2 increases (Figures 2e and 2g–2j), as seen in the linear progression of ΔT_s for forcings higher than 4×CO_2 for GISS-E2.1-G and 5×CO_2 for CESM-LE (Figures 1a and 1b). However, the NAWH temperature relative to ambient warming in the NH stays relatively constant. Note that the AMOC collapse in our models is by no means exceptional; for example, most CMIP5 and CMIP6 models also exhibit a substantial AMOC weakening in response to an abrupt quadrupling of CO_2 (Figures S3c and S3d).

The non-monotonicity of the response to increased CO_2 is not only seen in surface temperature: it pervades many aspects of the climate system. Consider the sea-ice response, shown in Figure 3 for both models. For GISS-E2.1-G, while the Arctic sea-ice decreases with CO_2 (Figure 3, left) at large concentrations, from 2× to 3×CO_2 sea-ice actually *increases* (Figure 3c) over the North Atlantic around Greenland and the Norwegian sea, consistent with a maximum NAWH temperature decrease at 3×CO_2 (Figure 2c). For CESM-LE, while Arctic sea-ice decreases with CO_2 (Figure 3, right) at large concentrations, from 3× to 4×CO_2 (Fig-

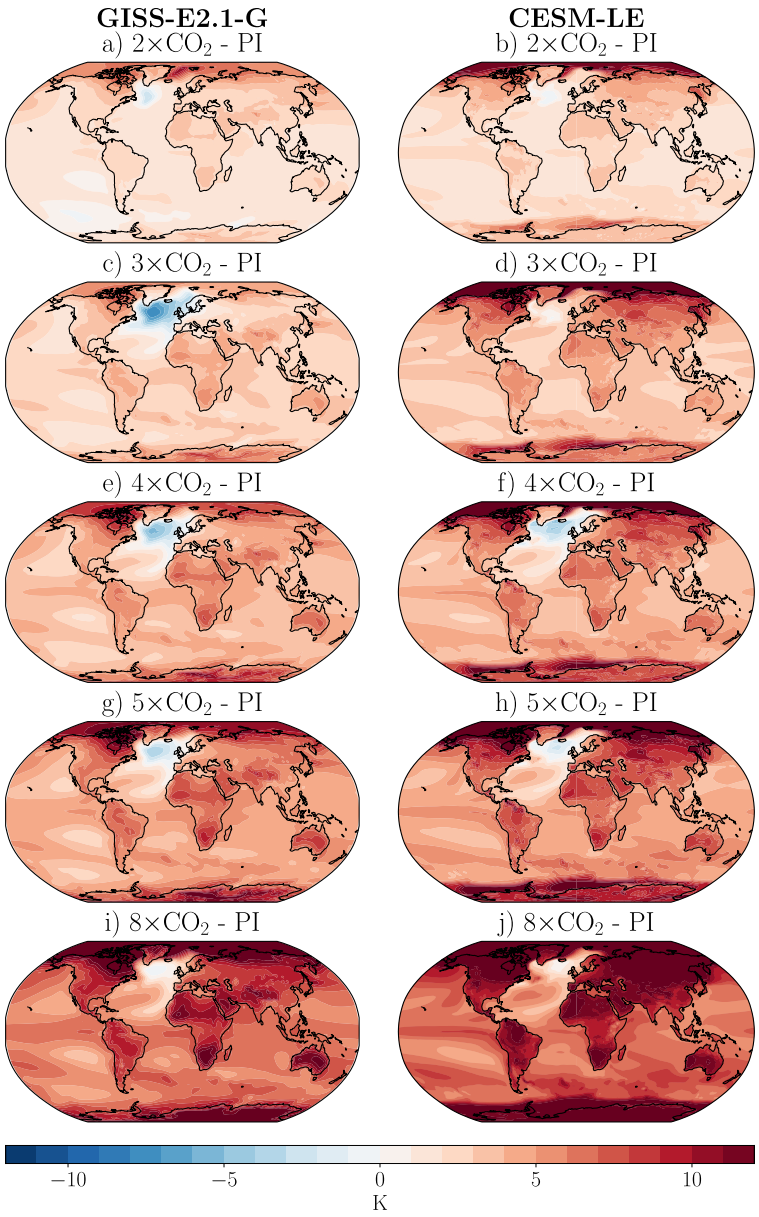

Figure 2. Annual mean surface temperature response (ΔT_s) to (a and b) 2×CO_2, (c and d) 3×CO_2, (e and f) 4×CO_2, (g and h) 5×CO_2, and (i and j) 8×CO_2 shown for both GISS-E2.1-G (left) and CESM-LE (right) model runs. Note: higher warming than 12K is shown with same color as 12K. CESM-LE, Community Earth System Model Large Ensemble; GISS-E2.1-G, Goddard Institute for Space Studies Model E2.1-G.

ures 3d and 3f) sea-ice actually *increases* (less red at 4×CO_2 than 3×CO_2). Furthermore, the non-monotonic response of Arctic sea-ice is not merely regional in scope: it is clearly seen in the annual NH sea-ice extent, which exhibits a significant "jump" between 2× and 3×CO_2 for GISS-E2.1-G and 3× and 4×CO_2 for CESM-LE shown in Figure 4a and Figure 4b, respectively. While numerous studies have explored the mechanisms by which Arctic sea-ice loss directly affects the behavior of the AMOC through increased freshwater fluxes (Liu et al., 2019; Oudar et al., 2017; Scinocca et al., 2009; Sévellec et al., 2017; Sun et al., 2018), here the relationship is not simply "one-way" as sea-ice *increases* between 2× to 3×CO_2 for GISS-E2.1-G, and between 3× to 4×CO_2 for CESM-LE, while the AMOC weakens. This is consistent with the fact that the physical processes associated with how sea-ice modulates the AMOC are still unclear in comprehensive fully coupled climate models (Liu et al., 2019). A detailed investigation of the relationship between Arctic ice

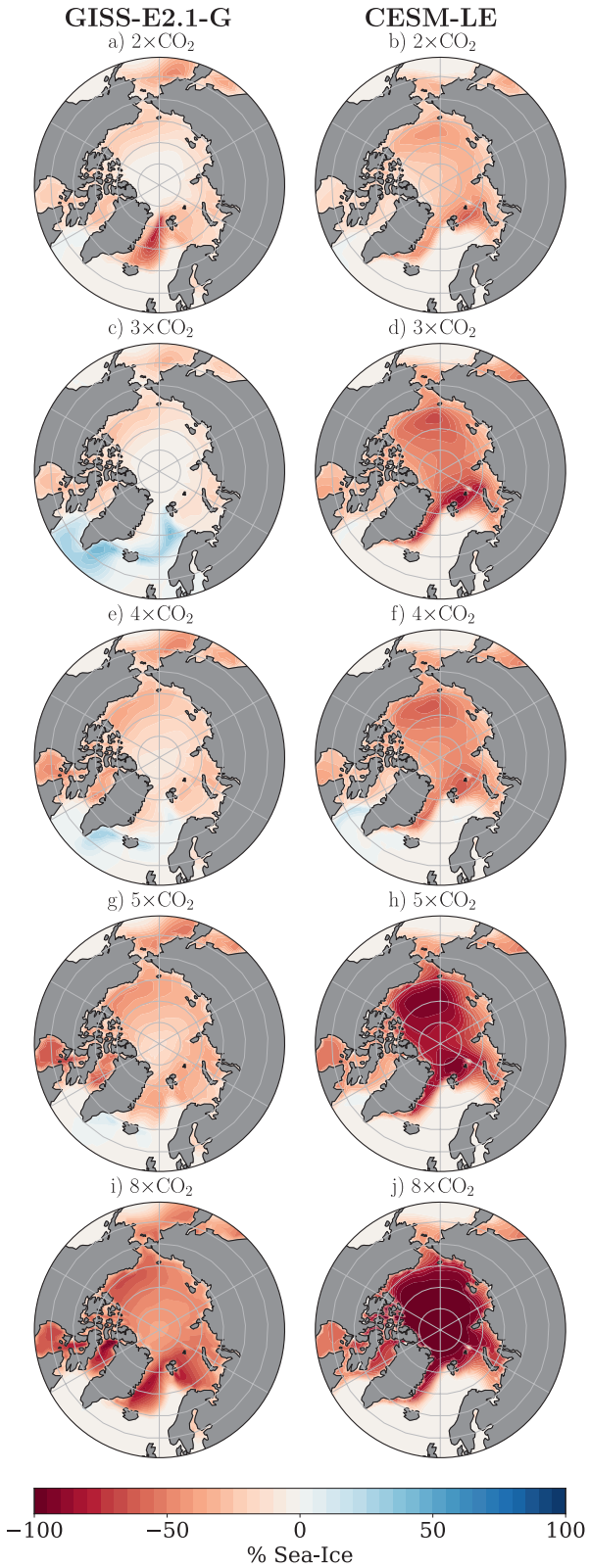

Figure 3. Annual Arctic sea-ice response to (a and b) 2×CO_2, (c and d) 3×CO_2, (e and f) 4×CO_2, (g and h) 5×CO_2, and (i and j) 8×CO_2 shown for both GISS-E2.1-G (left) and CESM-LE (right) model runs. CESM-LE, Community Earth System Model Large Ensemble; GISS-E2.1-G, Goddard Institute for Space Studies Model E2.1-G.

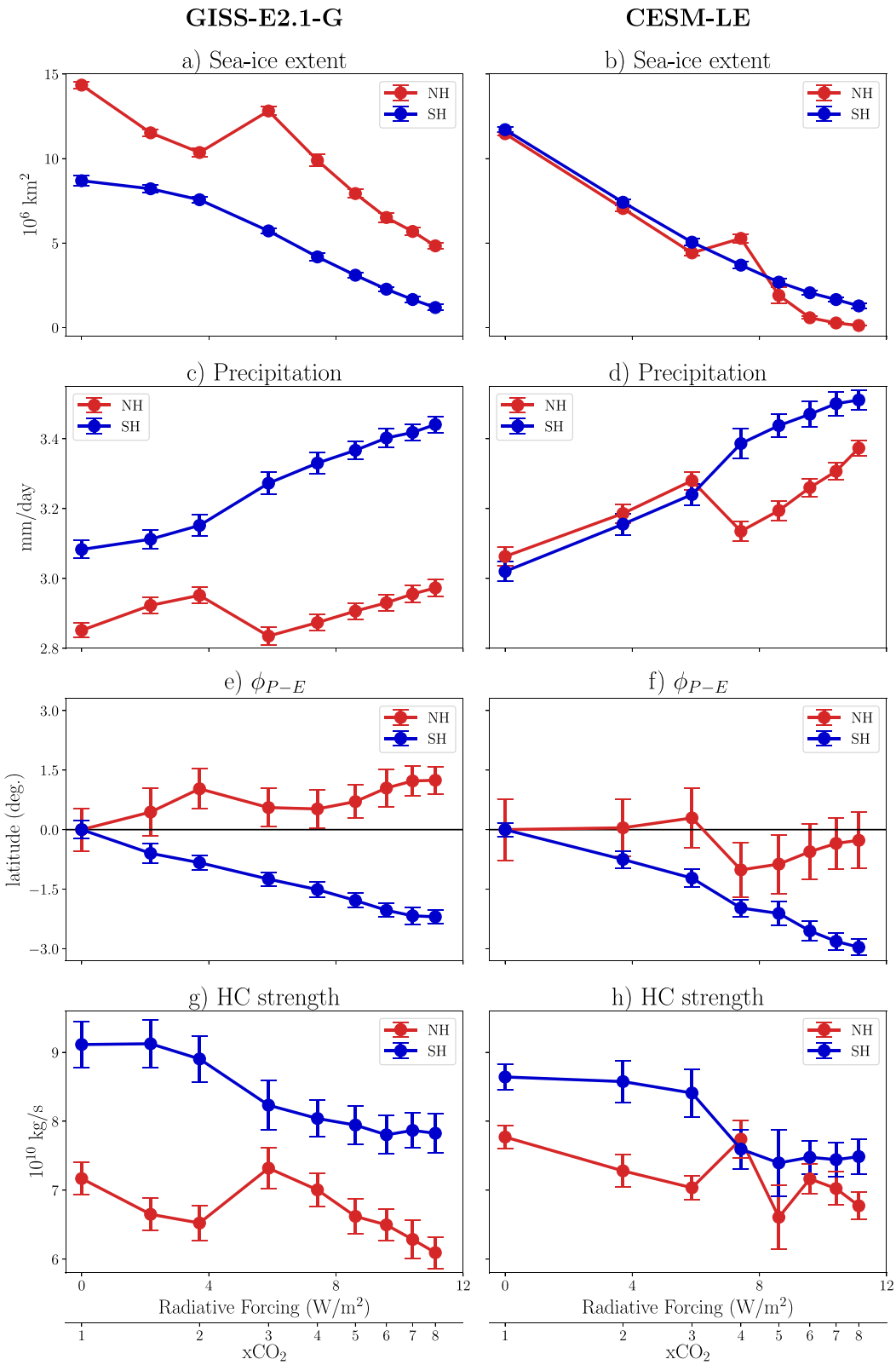

Figure 4. Annual mean (a and b) sea-ice extent (10^6 km^2) defined as grid cell areas with more than 15% ice concentration, (c and d) precipitation (mm/day), (e and f) dry zone edge (ϕ_{P-E}), and (g and h) HC strength (Ψ_{500}) for SH (blue) and NH (red) as a function of radiative forcing. Error bars denote 95% confidence intervals calculated using Student's *t*-distribution. HC, Hadley cell; SH, southern hemisphere.

and AMOC is beyond the scope of this study, but an analysis of the AMOC collapse in a previous generation of the GISS model (GISS-E2-G) can be found in Rind et al. (2018).

Many other climate variables also exhibit a non-monotonic response to increased CO_2 in both models. Of notable interest is the response of precipitation (Figures 4c and 4d), which generally increases in both hemispheres as CO_2 concentrations rise (as one expects), but actually declines in the NH (red line) between 2× and 3×CO_2 for GISS-E2.1-G, and between 3× and 4×CO_2 for CESM-LE, in tandem with temperature (Figures 1a and 1b) and sea-ice extent (Figures 4a and 4b). Interestingly, note that NH precipitation at 3×CO_2 in GISS-E2.1-G is lower than in the PI control (RF = 0) and barely recovers to its 2×CO_2 value even at 8×CO_2 forcing. Even in the SH, where precipitation increases monotonically, one can see a marked change in the slope between 2× and 3×CO_2 for GISS-E2.1-G, and between 3× and 4×CO_2 for CESM-LE. These features of the precipitation response are absent in the SOM runs (Figures S4a and S4b), and therefore, most likely are related to changes in the ocean dynamics.

The non-monotonic behavior is not confined to high or middle-latitude but extends to the tropics as well. The width of the tropical belt (Seidel et al., 2008), which is projected to increase with CO_2 (Chemke & Polvani, 2019; Grise et al., 2019), also exhibits a non-monotonic behavior. Consider the response of ϕ_{P-E} (Figures 4e and 4f), which is a critical metric of the hydrological cycle, separating zones of net precipitation and net evaporation. In the SH, ϕ_{P-E} shifts poleward with increased CO_2 in both models. On the other hand, in the NH, the models show a non-monotonic widening, with a contraction between 2× and 3×CO_2 in GISS-E2.1-G, and between 3× and 4×CO_2 in CESM-LE. By comparison, ϕ_{P-E} increases monotonically in the SOM runs in the NH (Figures S4c and S4d), which reinforces the notion that changes in ocean dynamics are important drivers of the non-monotonic climate response exhibited in these models.

The response of the edge of the dry zones (ϕ_{P-E}) is not only affected by atmospheric circulation changes but also by changes in moisture content, which is related to temperature, as shown in Chemke and Polvani (2019). Investigation of the moisture content in the NH (light blue line in Figures S5a and S5b) shows a clear "jump" between 2× and 3×CO_2 for GISS-E2.1-G, and between 3× and 4×CO_2 for CESM-LE, and confirms that changes in moisture content affect the response in ϕ_{P-E}, as one expects from the Clausius-Clapeyron relation and the temperature response shown in Figure 1.

Finally, we consider the strength of the HC, computed using the extremum of Ψ at 500 hPa (Ψ_{500}): it also exhibits a non-monotonic behavior in the NH, with a "jump" between 2× and 3×CO_2 in GISS-E2.1-G, and between 3× and 4×CO_2 in CESM-LE, as seen in Figures 4g and 4h, respectively (again, note that the "jump" disappears in the SOM runs, Figures S4e and S4f). A detailed study contrasting the different behaviors of various tropical width metrics is beyond the scope of this study. The goal of this paper is simply to illustrate that the non-monotonic response to increased CO_2 appears in a wide array of different metrics of the climate system.

4. Summary and Discussion

We have explored the climate system response to abrupt CO_2 forcing, spanning the range of 1× to 8×CO_2 using the GISS-E2.1-G and the CESM-LE models. We found that, in both models, for many climate metrics – ECS_{eff}, Arctic sea-ice, Northern Hemisphere precipitation, tropical expansion, and Hadley cell strength – the response to increased CO_2 is not only a non-linear but, in fact, a non-monotonic function of the RF. Our models show that increasing CO_2 from 2× to 3×PI concentrations in GISS-E2.1-G, and from 3× to 4×PI in CESM-LE model, results – surprisingly – in smaller ECS_{eff}, expanded Arctic sea-ice, reduced Northern hemisphere precipitation, contracted dry zones and a stronger Hadley cell. Analyzing a companion set of runs with the slab-ocean version of the same models reveals that this non-monotonic behavior is related to the changes in the ocean dynamics under CO_2 forcing.

Our findings are robust across two climate models for runs up to 150 years. It will be important to repeat a similar exercise with other climate models to determine if non-monotonicity is a robust feature, and not an artifact of the models used here. Additionally, it would be important to extend the model runs closer to equilibration (minimum of 1,000 years) and verify whether the monotonicity persists. We extended a subset of these integrations (2×, 3×, and 4×CO_2 with GISS-E2.1-G) for an additional 150 years, and our main results

are unchanged. More broadly, while the DECK experiments in CMIP at present only require a single abrupt (4×) CO_2 experiment, thereby limiting our ability to test for non-monotonicity using the CMIP output, our findings suggest that it may be important to explore a broader range of CO_2 forcings in future CMIPs.

Finally, one may ask whether the non-monotonicity of the response to CO_2 forcing detailed above is an artifact of the abrupt nature of the forcing. In practice, atmospheric concentrations of carbon dioxide increase progressively, and an abrupt change is highly unrealistic. Thus, in addition to validating the result presented here with other climate models, it will be essential to explore whether the non-monotonicity is also present in forced simulations with continuous forcing (e.g., 1% per year), and to determine whether the transient climate response also exhibits non-monotonic behavior. Such questions, of course, are beyond the scope of the present study, but we hope to report on them in future papers.

Data Availability Statement

The data used for the figures in the study is publicly available in a Zenodo repository at https://doi.org/10.5281/zenodo.3901624. The authors acknowledge the World Climate Research Programme's Working Group on Coupled Modeling and we thank all climate modeling groups for making available their model output.

Acknowledgments
This work was supported by NASA FINESST Grant 80NSSC20K1657. The work of LMP is supported, in part, by a grant from the US National Science Foundation to Columbia University. The authors thank the high-performance computing resources provided by NASA's Advanced Supercomputing (NAS) Division and the NASA Center for Climate Simulation (NCCS).

References

Ackerman, R., & Hegerl, G. C. (2008). The equilibrium sensitivity of the Earth's temperature to radiation changes. *Nature Geoscience*, *1*(11), 735–743. https://doi.org/10.1038/ngeo337

Adam, O., Grise, K. M., Staten, P., Simpson, I. R., Davis, S. M., Davis, N. A., et al. (2018). The tropd software package (v1): Standardized methods for calculating tropical-width diagnostics. *Geoscientific Model Development*, *11*(10), 4339–4357. https://doi.org/10.5194/gmd-11-4339-2018

Andrews, T., Timmermann, A., Tigchelaar, M., Elison Timm, O., & Ganopolski, A. (2016). Nonlinear climate sensitivity and its implications for future greenhouse warming. *Science Advances*, *2*(11), e1501923. https://doi.org/10.1126/sciadv.1501923

Arblaster, M., Schmidt, G. A., Nazarenko, L. S., Bauer, S. E., Ruedy, R., Russell, G. L., et al. (2020). GISS-E2.1: Configurations and climatology. *Journal of Advances in Modeling Earth Systems*, *12*(8). https://doi.org/10.1029/2019MS002025

Bauer, J. F., Reader, M. C., Plummer, D. A., Sigmond, M., Kushner, P. J., Shepherd, T. G., & Ravishankara, A. R. (2009). Impact of sudden Arctic sea-ice loss on stratospheric polar ozone recovery. *Geophysical Research Letters*, *36*(24). https://doi.org/10.1029/2009GL041239

Caballero, R., & Huber, M. (2013). State-dependent climate sensitivity in past warm climates and its implications for future climate projections. *Proceedings of the National Academy of Sciences*, *110*(35), 14162–14167. https://doi.org/10.1073/pnas.1303365110

Caesar, L., Rahmstorf, S., & Feulner, G. (2020). On the relationship between Atlantic meridional overturning circulation slowdown and global surface warming. *Environmental Research Letters*, *15*(2), 024003. https://doi.org/10.1088/1748-9326/ab63e3

Chemke, R., & Polvani, L. M. (2019). Exploiting the abrupt 4CO2 scenario to elucidate tropical expansion mechanisms. *Journal of Climate*, *32*(3), 859–875. https://doi.org/10.1175/JCLI-D-18-0330.1

Chemke, R., Zanna, L., & Polvani, L. M. (2020). Identifying a human signal in the North Atlantic warming hole. *Nature Communications*, *11*(1), 1540. https://doi.org/10.1038/s41467-020-15285-x

Colman, R., & McAvaney, B. (2009). Climate feedbacks under a very broad range of forcing. *Geophysical Research Letters*, *36*(1). https://doi.org/10.1029/2008GL036268

Forster, P. M., Richardson, T., Maycock, A. C., Smith, C. J., Samset, B. H., Myhre, G., et al. (2016). Recommendations for diagnosing effective radiative forcing from climate models for CMIP6. *Journal of Geophysical Research - D: Atmospheres*, *121*(20), 12460–12475. https://doi.org/10.1002/2016JD025320

Gregory, J. M., Andrews, T., & Good, P. (2015). The inconstancy of the transient climate response parameter under increasing CO2. *Phil. Trans. R. Soc. A.*, *373*(2054), 20140417. https://doi.org/10.1098/rsta.2014.0417

Gregory, J. M., Ingram, W. J., Palmer, M. A., Jones, G. S., Stott, P. A., Thorpe, R. B., et al. (2004). A new method for diagnosing radiative forcing and climate sensitivity. *Geophysical Research Letters*, *31*(3). https://doi.org/10.1029/2003GL018747

Grise, K. M., Davis, S. M., Simpson, I. R., Waugh, D. W., Fu, Q., Allen, R. J., et al. (2019). Recent tropical expansion: Natural variability or forced response? *Journal of Climate*, *32*(5), 1551–1571. https://doi.org/10.1175/JCLI-D-18-0444.1

Hegerl, L. B., Köhler, P., & Lohmann, G. (2019). Including the efficacy of land ice changes in deriving climate sensitivity from paleodata. *Earth System Dynamics*, *10*(2), 333–345. https://doi.org/10.5194/esd-10-333-2019

Holland, B., & Goldblatt, C. (2014). Radiative forcing at high concentrations of well-mixed greenhouse gases. *Geophysical Research Letters*, *41*(1), 152–160. https://doi.org/10.1002/2013GL058456

Jonko, A. K., Shell, K. M., Sanderson, B. M., & Danabasoglu, G. (2013). Climate feedbacks in CCSM3 under changing CO2 forcing. part II: Variation of climate feedbacks and sensitivity with forcing. *Journal of Climate*, *26*(9), 2784–2795. https://doi.org/10.1175/JCLI-D-12-00479.1

Kay, J. E., Deser, C., Phillips, A., Mai, A., Hannay, C., Strand, G., et al. (2015). The community earth system model (CESM) large ensemble project: A community resource for studying climate change in the presence of internal climate variability. *Bulletin of the American Meteorological Society*, *96*(8), 1333–1349. https://doi.org/10.1175/BAMS-D-13-00255.1

Knutti, R., Rugenstein, M. A. A., & Hegerl, G. C. (2017). Beyond equilibrium climate sensitivity. *Nature Geoscience*, *10*(10), 727–736. https://doi.org/10.1038/ngeo3017

Kröger, M. A., Foster, G. L., Chalk, T. B., Rohling, E. J., Sexton, P. F., Lunt, D. J., et al. (2015). Plio-pleistocene climate sensitivity evaluated using high-resolution CO2 records. *Nature*, *518*(7537), 49–54. https://doi.org/10.1038/nature14145

Levine, X. J., & Schneider, T. (2011). Response of the Hadley circulation to climate change in an aquaplanet GCM coupled to a simple representation of ocean heat transport. *Journal of the Atmospheric Sciences*, *68*(4), 769–783. https://doi.org/10.1175/2010JAS3553.1

Liu, W., Fedorov, A., & Sévellec, F. (2019). The mechanisms of the Atlantic meridional overturning circulation slowdown induced by Arctic sea ice decline. *Journal of Climate*, *32*(4), 977–996. https://doi.org/10.1175/JCLI-D-18-0231.1

Maher, N., Milinski, S., Suarez-Gutierrez, L., Botzet, M., Dobrynin, M., Kornblueh, L., et al. (2019). The Max Planck institute grand ensemble: Enabling the exploration of climate system variability. *Journal of Advances in Modeling Earth Systems*, *11*(7), 2050–2069. https://doi.org/10.1029/2019MS001639

Meraner, K., Mauritsen, T., & Voigt, A. (2013). Robust increase in equilibrium climate sensitivity under global warming. *Geophysical Research Letters*, *40*(22), 5944–5948. https://doi.org/10.1002/2013GL058118

O'Gorman, P. A., & Schneider, T. (2008). The hydrological cycle over a wide range of climates simulated with an idealized GCM. *Journal of Climate*, *21*(15), 3815–3832. https://doi.org/10.1175/2007JCLI2065.

Oudar, T., Sanchez-Gomez, E., Chauvin, F., Cattiaux, J., Terray, L., & Cassou, C. (2017). Respective roles of direct GHG radiative forcing and induced Arctic sea ice loss on the northern hemisphere atmospheric circulation. *Climate Dynamics*, *49*(11), 3693–3713. https://doi.org/10.1007/s00382-017-3541-0

Palter, J. B. (2015). The role of the Gulf Stream in European climate. *Annual Reviews of Marine Science*, *7*(1), 113–137. https://doi.org/10.1146/annurev-marine-010814-015656

Pancost, K., Pincus, R., Schmidt, G. A., & Miller, R. L. (2018). Internal variability and disequilibrium confound estimates of climate sensitivity from observations. *Geophysical Research Letters*, *45*(3), 1595–1601. https://doi.org/10.1002/2017GL076468

Rind, D., Schmidt, G. A., Jonas, J., Miller, R., Nazarenko, L., Kelley, M., & Romanski, J. (2018). Multicentury instability of the Atlantic meridional circulation in rapid warming simulations with GISS ModelE2. *Journal of Geophysical Research-D: Atmospheres*, *123*(12), 6331–6355. https://doi.org/10.1029/2017JD027149

Rosenlof, K. M., & Polvani, L. M. (2016). Is climate sensitivity related to dynamical sensitivity? *Journal of Geophysical Research - D: Atmospheres*, *121*(10), 5159–5176. https://doi.org/10.1002/2015JD024687

Rugenstein, M. A. A., Winton, M., Stouffer, R. J., Griffies, S. M., & Hallberg, R. (2013). Northern high-latitude heat budget decomposition and transient warming. *Journal of Climate*, *26*(2), 609–621. https://doi.org/10.1175/JCLI-D-11-00695.1

Schmidt, G. A., Ruedy, R., Hansen, J. E., Aleinov, I., Bell, N., Bauer, M., et al. (2006). Present-day atmospheric simulations using GISS ModelE: Comparison to in situ, satellite, and reanalysis data. *Journal of Climate*, *19*(2), 153–192. https://doi.org/10.1175/JCLI3612.1

Seidel, D. J., Fu, Q., Randel, W. J., & Reichler, T. J. (2008). Widening of the tropical belt in a changing climate. *Nature Geoscience*, *1*(1), 21. https://doi.org/10.1038/ngeo.2007.38

Sévellec, F., Fedorov, A. V., & Liu, W. (2017). Arctic sea-ice decline weakens the Atlantic Meridional Overturning Circulation. *Nature Climate Change*, *7*(8), 604–610. https://doi.org/10.1038/nclimate3353

Shaffer, G., Huber, M., Rondanelli, R., & Pepke Pedersen, J. O. (2016). Deep time evidence for climate sensitivity increase with warming. *Geophysical Research Letters*, *43*(12), 6538–6545. https://doi.org/10.1002/2016GL069243

Sherwood, S. C., Bony, S., Boucher, O., Bretherton, C., Forster, P. M., Gregory, J. M., & Stevens, B. (2015). Adjustments in the forcing-feedback framework for understanding climate change. *Bulletin of the American Meteorological Society*, *96*(2), 217–228. https://doi.org/10.1175/BAMS-D-13-00167.1

Sherwood, S. C., Webb, M. J., Annan, J. D., Armour, K. C., Forster, P. M., Hargreaves, J. C., et al. (2020). An assessment of Earth's climate sensitivity using multiple lines of evidence. *Review of Geophysics*, *58*. https://doi.org/10.1029/2019RG000678

Sun, L., Alexander, M., & Deser, C. (2018). Evolution of the global coupled climate response to Arctic Sea ice loss during 1990-2090 and its contribution to climate change. *Journal of Climate*, *31*(19), 7823–7843. https://doi.org/10.1175/JCLI-D-18-0134.1

Tian, B. (2015). Spread of model climate sensitivity linked to Double-Intertropical Convergence Zone bias. *Geophysical Research Letters*, *42*(10), 4133–4141. https://doi.org/10.1002/2015GL064119

Trossman, D. S., Palter, J. B., Merlis, T. M., Huang, Y., & Xia, Y. (2016). Large-scale ocean circulation-cloud interactions reduce the pace of transient climate change. *Geophysical Research Letters*, *43*(8), 3935–3943. https://doi.org/10.1002/2016GL067931

Waugh, C. M., Shell, K. M., Gent, P. R., Bailey, D. A., Danabasoglu, G., Armour, K. C., et al. (2012). Climate sensitivity of the community climate system model, version 4. *Journal of Climate*, *25*(9), 3053–3070. https://doi.org/10.1175/jcli-d-11-00290.1

Winton, M., Griffies, S. M., Samuels, B. L., Sarmiento, J. L., & Frölicher, T. L. (2013). Connecting changing ocean circulation with changing climate. *Journal of Climate*, *26*(7), 2268–2278. https://doi.org/10.1175/JCLI-D-12-00296.1

Zelinka, M. D., Myers, T. A., McCoy, D. T., Po-Chedley, S., Caldwell, P. M., Ceppi, P., et al. (2020). Causes of higher climate sensitivity in CMIP6 models. *Geophysical Research Letters*, *47*(1). https://doi.org/10.1029/2019GL085782